Local and Spatial Disorder in β''-$(ET)_2SF_5RSO_3$ Solid Solutions (R = CH_2CF_2, CHF, $CHFCF_2$)

A. D. Garlach and J. L. Musfeldt*

Department of Chemistry, University of Tennessee, Knoxville, Tennessee 37932

J. M. Pigos and B. R. Jones

Department of Chemistry, State University of New York at Binghamton, Binghamton, New York 13902-6016

I. Olejniczak and A. Graja

Institute of Molecular Physics, Polish Academy of Sciences, Poznan, Poland

M.-H. Whangbo

Department of Chemistry, North Carolina State University, Raleigh, North Carolina 27695-8204

J. A. Schlueter and U. Geiser

Chemistry and Materials Science Divisions, Argonne National Laboratory, Argonne, Illinois 60439

R.W. Winter and G.L. Gard

Department of Chemistry, Portland State University, Portland, Oregon 97207-0751

Received November 29, 2001. Revised Manuscript Received April 22, 2002

We report the polarized infrared reflectance spectra and optical conductivity of β''-$(ET)_2SF_5RSO_3$ superconducting (R = CH_2CF_2), metallic (R = CHF), and metal−insulator (R = $CHFCF_2$) mixed crystal materials. Incorporation of chiral counterions in the superconducting matrix allows us to tune the physical and spectroscopic properties over the composition range by modulating the anion potential. We conclude that the two low-energy electronic excitations at ≈5200 and 9600 cm^{-1} are spectral manifestations of charge localization in the ET stack, made manifest by both local (anion pocket) and spatial (positional) disorder.

Introduction

Disorder is a well-known rival of superconductivity, as found for a variety of materials in a number of different forms. Examples include crystallographic disorder, solvent disorder, radiation-induced disorder, localization disorder, thermal disorder, cooling-rate-induced disorder, structural disorder due to composition changes, orientational disorder by chemical design, and magnetic disorder,[1−13] to name but a few. The effect of various types of disorder on molecular superconductors has been an area of particular interest ever since superconductivity was observed in these systems.[3,7,14−30]

(1) Wang, H. H.; Kini, A. M.; Montgomery, L. K.; Geiser, U.; Carlson, K. D.; Williams, J. M.; Thompson, J. E.; Watkins, D. M.; Kwok, W. K.; Welp, U.; Vandervoort, K. G. *Chem. Mater.* **1990**, *2*, 482.
(2) Schlueter, J. A.; Geiser, U.; Wang, H. H.; Kelly, M. E.; Dudek, J. D.; Williams, J. M.; Naumann, D.; Roy, T. *Mol. Cryst. Liq. Cryst.* **1996**, *284*, 195.
(3) Olejniczak, I.; Graja, A.; Brau, A.; Farges, J. P.; Dupuis, P. *Phys. Status Solidi* **1994**, *145*, 197.
(4) TrÆtteberg, O. Ph.D. Thesis, University of Paris-Sud, Centre D'Orsay, France, 1993.
(5) Burgin, T.; Miebach, T.; Huffman, J. C.; Montgomery, L. K.; Paradis, J. A.; Rovira, C.; Whangbo, M. H.; Magonov, S. N.; Khan, S. I.; Strouse, C. E.; Overmyer, D. L.; Schirber, J. E. *J. Mater. Chem.* **1995**, *5*, 1659.
(6) Ishiguro, T.; Yamaji, K.; Saito, G. In *Organic Superconductors*; Fulde, P., Ed.; Springer: Berlin, 1990.
(7) Drozdova, O.; Saito, G.; Yamochi, H.; Ookubo, K.; Yakushi, K.; Uruichi, M.; Ouahab, L. *Inorg. Chem.* **2001**, *40*, 3265.
(8) Ozturk, T.; Saygili, N.; Ozkara, S.; Pilkington, M.; Rice, C. R.; Tranter, D. A.; Turksoy, F.; Wallis, J. D. *J. Chem. Soc., Perkin Trans. 1* **2001**, *4*, 407.
(9) He, T.; Cava, R. J. *Phys. Rev. B* **2001**, *63*, 172403.
(10) Teklu, A. A.; Goodrich, R. G.; Harrison, N.; Hall, D.; Fisk, Z.; Young, D. *Phys. Rev. B* **2000**, *62*, 12875.
(11) Reddy, B. V.; Jena, P.; Deevi, S. C. *Intermetallics* **2000**, *8*, 1197.
(12) Miyasaka, S.; Takagi, H.; Sekine, Y.; Takahashi, H.; Mori, N.; Cava, R. J. *J. Phys. Soc. Jpn.* **2000**, *69*, 3166.
(13) Slusky, J. S.; Rogado, N.; Regan, K. A.; Hayward, M. A.; Khalifah, P.; He, T.; Inumaru, K.; Loureiro, S. M.; Haas, M. K.; Zandbergen, H. W.; Cava, R. J. *Nature* **2001**, *410*, 343.
(14) Garoche, P.; Brusetti, R.; Bechgaard, K. *Phys. Rev. Lett.* **1982**, *49*, 1346.
(15) Coulon, C.; Delhaes, P.; Amiell, J.; Manceau, J. P.; Fabre, J. M.; Giral, L. *J. Phys. (Paris)* **1982**, *43*, 1721.
(16) Park, J. H.; Choi, S. J.; Kang, W. *Synth. Met.* **1999**, *103* 2121.
(17) Emge, T. J.; Wang, H. H.; Beno, M. A.; Leung, P. C. W.; Firestone, M. A.; Jenkins, H. C.; Cook, J. D.; Carlson, K. D.; Williams, J. M.; Venturini, E. L.; Azevedo, L. J.; Schirber, J. E. *Inorg. Chem.* **1985**, *24*, 1736.
(18) Forro, L.; Bouffard, S.; Schweitzer, D. *Solid State Commun.* **1988**, *65*, 1359.

10.1021/cm010378b CCC: $22.00
Published on Web 06/21/2002

For instance, the superconducting state of the first ambient pressure molecular superconductor, $(TMTSF)_2ClO_4$, where TMTSF is tetramethyltetraselenalfulvalene, is suppressed by anion disorder created by thermal quenching, defects induced by doping with small amounts of TMTTF, and to a lesser extent by radiation damage to the conducting chains.[14−16] More recently, the superconducting transition temperature of the intriguing κ-$(ET)_2Cu^{+}_{(2-x-y)}Cu^{2+}_{x}(CN)_{(3-2y)}[N(CN)_2]_y$ system, where ET refers to BEDT-TTF or bis(ethylenedithio)tetrathiafulvalene), can be tuned between 3.2 and 10 K by adjusting the x and y parameters.[7,31] Various types of imperfections cause disorder over different length scales. Radiation-induced disorder creates large length-scale damage, crystallographic disorder and alloying create medium-length irregularities, and solvent and orientational disorder result in localized, molecular-scale disorder. The effects of disorder are evident in key physical properties such as the lowering of a superconducting transition temperature, T_c, and the broadening of vibrational modes in an infrared spectrum.[3,32]

Among the organic solids, the β''-$(ET)_2SF_5RSO_3$ family of materials has attracted attention because of the tunable nature of the counterion and the different ground states that are observed in this system.[33−38] In the β'' system, R = CH_2CF_2, CHF, and $CHFCF_2$ yield superconducting ($T_c \sim 5.2$ K), metallic, and metal−insulator materials, respectively.[26,33,36,38,39] Extensive spectroscopic studies of these isostructural compounds have identified two large, low-energy electronic excitations (centered at ≈5200 and 9600 cm^{-1}) in the metal−insulator (R = $CHFCF_2$) material, which were attributed to either correlation-driven or disorder-related localization.[35,36,40]

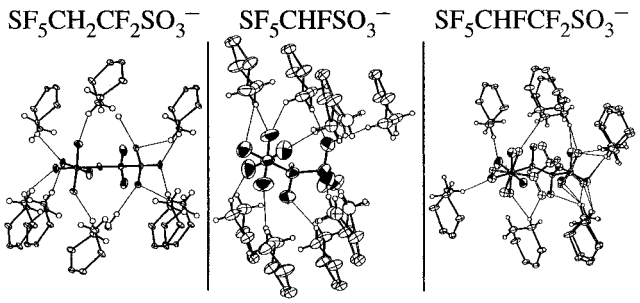

Figure 1. Hydrogen-rich anion cavities of β''-$(ET)_2SF_5CH_2CF_2SO_3$ (left), β''-$(ET)_2SF_5CHFSO_3$ (center), and β''-$(ET)_2SF_5CHFCF_2SO_3$ (right). The outer six-membered rings of the ET molecules are shown. Short hydrogen-bonding contacts are observed between the hydrogen atoms of the ET molecules and the electronegative fluorine and oxygen atoms of the anion. In the case of β''-$(ET)_2SF_5CHFCF_2SO_3$, hydrogen-bonding competition for the CF fluorine atom induces anion disorder.

To probe the origin of the low-energy electronic excitations in the β''-$(ET)_2SF_5RSO_3$ family of organic solids, we prepared a series of superconductor/metallic (SC/M) and superconductor/metal−insulator (SC/MI) solid solutions. These anions were chosen because we wanted to tune the SC with anions that form isostructural salts.[41] In such mixed crystals, there are two very different types of disorder: spatial and local disorder. Spatial disorder occurs over an intermolecular length scale because of positional variation of different anions.[42] It is present in both the SC/M and SC/MI composites. Local disorder is different and occurs over a smaller length scale. In β''-$(ET)_2SF_5CHFCF_2SO_3$, it occurs inside the anion pocket and affects the hydrogen bonding between the $SF_5RSO_3^-$ anion and the ethylene groups on the ET molecules, as shown in Figure 1.[36] This disruption occurs in the SC/MI composites (and the pristine MI material itself) because of a random mixture of enantiomers in the structure at the MI site. It is not present in the SC/M composites because both anions are ordered. To summarize, the SC/M alloys contain only long-range spatial disorder, and the SC/MI composites display both spatial and local disorder. Table 1 lists the characteristic features for each system.

The overall goal of the present work is to pinpoint the microscopic origin of the aforementioned low-energy electronic excitations in the β''-$(ET)_2SF_5RSO_3$ system by investigating the spectroscopic response of a series of mixed crystals. We employ different anion types to tune the physical and spectroscopic properties smoothly across composition space, and in so doing, we conclu-

(19) Tokumoto, M.; Anzai, H.; Murata, K.; Kajimura, K.; Ishiguro, T. *Synth. Met.* **1988**, *27*, A251.
(20) Muller, J.; Lang, M.; Steglich, F.; Schlueter, J. A.; Kini, A. M.; Sasaki, T. *Phys. Rev. B.* **2002**, *65*, 144521.
(21) Akutsu, H.; Saito, K.; Sorai, M. *Phys. Rev. B* **1999**, *61*, 4346.
(22) Tokumoto, M.; Kinoshita, N.; Tanaka, Y.; Kinoshita, T.; Anzi, H. *Synth. Met.* **1999**, *103*, 1971.
(23) Su, X.; Zuo, F.; Schlueter, J. A.; Kelly, M. E.; Williams, J. M. *Solid State Commun.* **1998**, *107*, 731.
(24) Naito, T.; Miyamoto, A.; Kobayashi, H.; Kato, R.; Kobayashi, A. *Chem. Lett.* **1992**, 119.
(25) Kushch, N. D.; Buravov, L. I.; Khomenko, A. G.; Yagubskii, E. B.; Rosenberg, L. P.; Shibaeva, R. P. *Synth. Met.* **1993**, *53*, 155.
(26) Geiser, U.; Schlueter, J. A.; Wang, H. H.; Williams, J. M.; Nauman, D.; Roy, T. *Acta Crystallogr. B* **1995**, *51*, 789.
(27) Schlueter, J. A.; Geiser, U.; Kini, A. M.; Wang, H. H.; Williams, J. M.; Naumann, D.; Roy, T.; Hoge, B.; Eujen, R. *Coord. Chem. Rev.* **1999**, *190−192*, 781.
(28) Tanaka, H.; Kobayashi, A.; Saito, T.; Kawano, K.; Naito, T.; Kobayashi, H. *Adv. Mater.* **1996**, *8*, 812.
(29) Kobayashi, H.; Akutsu, H.; Arai, E.; Tanaka, H.; Kobayashi, A. *Phys. Rev. B.* **1997**, *56*, R8526.
(30) Kobayashi, H.; Sato, A.; Arai, E.; Akutsu, H.; Kobayashi, A.; Cassoux, P. *J. Am. Chem. Soc.* **1997**, *119*, 12392.
(31) This material was previously called κ'-$(ET)_2Cu_2(CN)_3$.
(32) Monteverde, M.; Nenez-Regueiro, M.; Rogado, N.; Regan, K. A.; Hayward, M. A.; He, T.; Loureiro, S. M.; Cava, R. J. *Science* **2001**, *292*, 75.
(33) Ward, B. H.; Schlueter, J. A.; Geiser, U.; Wang, H. H.; Morales, E.; Parakka, J.; Thomas, S. Y.; Williams, J. M.; Nixon, P. G.; Winter, R. W.; Gard, G. L.; Koo, H. J.; Whangbo, M. H. *Chem. Mater.* **2000**, *12*, 343.
(34) Dong, J.; Musfeldt, J. L.; Schlueter, J. A.; Williams, J. M.; Nixon, P. G.; Winter, R. W.; Gard, G. L. *Phys. Rev. B* **1999**, *60*, 4342.
(35) Olejniczak, I.; Jones, B. R.; Zhu, Z.; Dong, J.; Musfeldt, J. L.; Schlueter, J. A.; Morales, E.; Geiser, U.; Nixon, P. G.; Winter, R. W.; Gard, G. L. *Chem. Mater.* **1999**, *11*, 3160.
(36) Jones, B. R.; Olejniczak, I.; Dong, J.; Pigos, J. M.; Zhu, Z. T.; Garlach, A. D.; Musfeldt, J. L.; Koo, H.-J.; Whangbo, M.-H.; Schlueter, J. A.; Ward, B. H.; Morales, E.; Kini, A. M.; Winter, R. W.; Mohtasham, J.; Gard, G. L. *Chem. Mater.* **2000**, *12*, 2490.
(37) Geiser, U.; Schlueter, J. A.; Wang, H. H.; Kini, A. M.; Williams, J. M.; Sche, P. P.; Zakowicz, H. I.; VanZile, M. L.; Dudek, J. D.; Nixon, P. G.; Winter, R. W.; Gard, G. L.; Ren, J.; Whangbo, M.-H. *J. Am. Chem. Soc.* **1996**, *118*, 9996.
(38) Schlueter, J. A.; Ward, B. H.; Geiser, U.; Wang, H. H.; Kini, A. M.; Parakka, J.; Morales, E.; Koo, H. J.; Whangbo, M. H.; Winter, R. W.; Mohtasham, J.; Gard, G. L. *J. Mater. Chem.* **2001**, *11*, 2008.

(39) β''-$(ET)_2SF_5CHFCF_2SO_3$ displays a weak first-order transition near 175 K. The variable temperature dc resistivity is low and "metallic" about the transition temperature; it displays a semiconducting temperature dependence below 175 K.[35]
(40) Slight hints of the 5200-cm^{-1} excitation are also observed in the spectra of the superconducting and metallic materials; the 9600-cm^{-1} feature is present only in the metallic sample (R = CHF).[36]
(41) We did not, for instance, use $SF_5CF_2SO_3^-$ because it forms a β' structure. Although the $SF_5CH_2SO_3^-$ anion forms a β'' structure, the symmetry is different, with alternating stacks.[33]
(42) In this case, both random (e.g., ACACCACA) and ordered (e.g., $A_nC_mA_nC_m$) anion arrangements are possible.

Table 1. Different Forms of Spatial and Local Disorder for the Pristine Compounds and the Superconductor/Metal (SC/M) and Superconductor/Metal−Insulator (SC/MI) Composites of the β″-(ET)$_2$SF$_5$RSO$_3$ System[a]

anion arrangement	SC	M	MI (local anion pocket disorder)	SC/M (long-range positional disorder only)	SC/MI (combined long-range positional and local anion pocket disorder)
random				ACCACAAC	AB*B*AB*AAB*
ordered (alternating)				ACACACAC	AB*AB*AB*AB*
ordered (block)	AAAAAA	CCCCCC	B*B*B*B*B*B*	$(A)_n(C)_m(A)_n(C)_m$	$(A)_n(B^*)_m(A)_n(B^*)_m$
summary of optical properties results	very weak excitation at 5200 cm^{-1}	weak excitations at 5200 and 9600 cm^{-1}	very strong excitations at 5200 and 9600 cm^{-1}	varible intensity excitations at 5200 and 9600 cm^{-1}	varible intensity excitations at 5200 and 9600 cm^{-1}

[a] Asterisk indicates local (anion pocket) disorder. A = superconductor anion (R = CH_2CF_2), B = metal/insulator anion (R = $CHFCF_2$), and C = metal anion (R = CHF).

sively prove that the aforementioned low-energy excitations at 5200 and 9600 cm^{-1} are spectroscopic manifestations of both spatial and local disorder.

II. Experimental Section

Single crystals of pure β″-(ET)$_2$SF$_5$CH$_2$CF$_2$SO$_3$ (SC), β″-(ET)$_2$SF$_5$CHFSO$_3$ (M), and β″-(ET)$_2$SF$_5$CHFCF$_2$SO$_3$ (MI), and the β″-(ET)$_2$(SF$_5$CH$_2$CF$_2$SO$_3$)$_{1-x}$(SF$_5$CHFSO$_3$)$_x$ (SC/M) and β″-(ET)$_2$(SF$_5$CH$_2$CF$_2$SO$_3$)$_{1-x}$(SF$_5$CHFCF$_2$SO$_3$)$_x$ (SC/MI) composites were grown by electrocrystallization techniques analogous to those described previously.[33] All crystals were grown from 1,1,2-trichloroethane solutions containing 12-crown-4 and the lithium salts of the desired anion.

The composites were crystallized from an electrolyte solution containing the desired molar ratio of anions. On the basis of both our dc resistivity and X-ray structure data, we estimate that composite compositions are accurate to better than ±5%, more than sufficient for our purposes, as detailed below. Although all circumstantial evidence suggests a statistical distribution of counterions with the composition of the original solution, it was not possible to directly confirm that the anion composition in the crystallized salt was identical to the composition of the mother liquid through elemental analysis or EDAX techniques because of the nearly identical elemental composition of the anions in the solid solutions.

Single-crystal X-ray diffraction results on the pure SC, M, and MI compounds have been previously reported.[33,37,38] X-ray results on the composites[43] indicate that unit cell parameters vary smoothly with doping between the pure compound limits. Moreover, the unit cells of different crystals within a single batch show uniform parameters, indicating similar dopant levels. For the case of the SC/M composites, the aforementioned trend is seen most clearly in a plot of the relative change of the unit cell angles with dopant level (Figure 2). The case of the SC/MI alloys is more complex, but the unit cell variation is consistent with a composite composition similar to the molar ratio of anions used in the crystallization solution. At 300 K, unit cell parameters vary smoothly with dopant level (not shown), as is the case when $SF_5CHFSO_3^-$ is used as the dopant. However, at low temperature (150 K), a crossover is observed from a metallic state, at dopant level $x = 0.5$, to the insulating state at $x = 0.75$ (Figure 2). The MI transition, which we previously reported near 200 K for β″-(ET)$_2$SF$_5$CHFCF$_2$SO$_3$ [35,38] is clearly observed in the temperature variation of unit cell parameters, most obviously in the *a* and *b*-axis lengths and the β angle (Figure 2).[44] Variable temperature X-ray studies indicate that the MI transition temperature increases as the dopant level of $SF_5CHFCF_2SO_3^-$ increases. Thus, although the exact mixed crystal compositions are not known precisely, the uncertainties in the dopant levels are smaller than the incremental increases in dopant level reported in this paper (100:0, 75:25, 50:50, 25:75, and 0:100 for both SC/M and SC/MI composites, respectively).

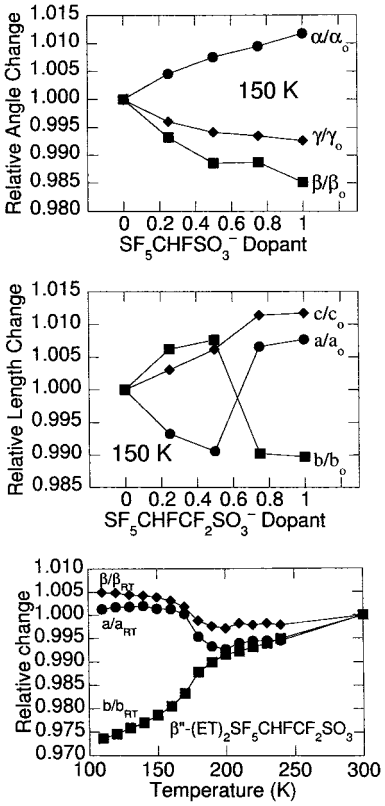

Figure 2. (a) Unit cell angles at 150 K as a function of dopant level in the β″-(ET)$_2$ (SF$_5$CH$_2$CF$_2$SO$_3$)$_{1-x}$(SF$_5$CHFSO$_3$)$_x$ system, illustrating a smooth variation of unit cell as a function of dopant level. (b) Unit cell parameters of the β″-(ET)$_2$(SF$_5$CH$_2$CF$_2$SO$_3$)$_{1-x}$(SF$_5$CHFCF$_2$SO$_3$)$_x$ system as a function of dopant level at 150 K. At this temperature, the β″-(ET)$_2$SF$_5$CH$_2$CF$_2$SO$_3$ and β″-(ET)$_2$(SF$_5$CH$_2$CF$_2$SO$_3$)$_{0.25}$(SF$_5$CHFCF$_2$SO$_3$)$_{0.75}$ samples are below the MI transition. (c) Relative change of the unit cell parameters of β″-(ET)$_2$SF$_5$CHFCF$_2$SO$_3$ as a function of temperature. The metal-to-insulator transition is clearly visible near 200 K.

Figure 3 displays the resistivity data[45] for the pure materials and the 50:50 SC/M and SC/MI mixed crystals as a function of temperature. The 50:50 SC/M composite has resistivity behavior very similar to that of the M compound. The resistivity of the 50:50 SC/MI sample is similar to that of the MI material, except that the transition temperature is shifted about 40 K lower. On the basis of both the X-ray and dc resistivity results, we estimate that the alloy concentration is

(43) Single-crystal X-ray diffraction data were collected on a SMART single-crystal X-ray diffractometer equipped with a CCD-based area detector and a sealed tube X-ray source.

(44) The MI transition does not significantly influence the optical response.[35]

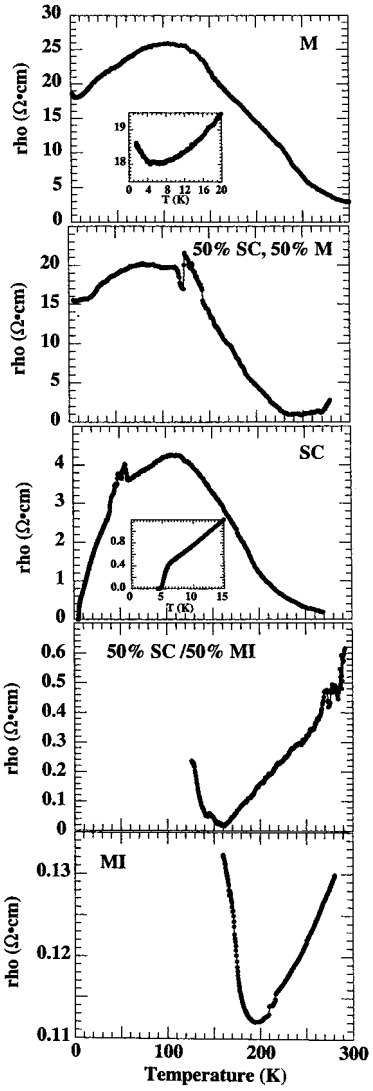

Figure 3. Temperature dependence of the electrical resistivity measured for single-crystal samples of the pure SC, M, and MI materials and the two 50:50 mixed crystals. Note that the small discontinuities and noise in the data likely result from contact problems to the sample and does not represent a true variation in the resistivity.

known to within at least 5%, more than sufficient for our purposes.

Polarized middle and near-infrared reflectance measurements were performed on a Bruker 55 Equinox spectrometer equipped with an infrared microscope (IR Scope II).[46] We covered the 600−12500-cm^{-1} regime. Nitrogen-cooled detectors (MCT and InSb) and standard polarizers were used as appropriate. The optical axes of the crystal were determined as those displaying the greatest anisotropy at 300 K, and analysis of the structure shows good correspondence with the $\vec{E} \parallel b$ and $\vec{E} \perp b$ directions. All data were collected at 300 K. The optical constants were obtained from a Kramers−Kronig analysis of the reflectance spectra, as described previously.[36]

(45) Temperature-dependent electrical resistivity measurements of the pure salts and the 50:50 alloys were made using a four-probe dc technique with a Lakeshore model 7000 cryostat equipped with RES7000 software. The linearly arranged current and voltage contacts were made with gold wire (0.0005 in diameter) attached directly to the crystals with fast-drying silver paint (DuPont). Resistivity data were recording during both cooling and warming cycles, and a slow cooling/warming rate of about 1 K/min was used to prevent microcracking of either the crystal of the contacts. A direct current of 1 mA was applied.

(46) The dimensions of the single crystals used for infrared measurements were ≈1.9 × 0.7 × 0.4 mm.

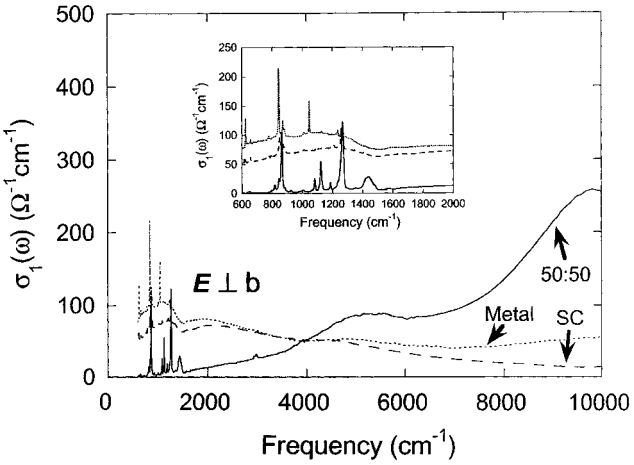

Figure 4. 300 K optical conductivity of the β''-$(ET)_2SF_5CH_2CF_2SO_3$ superconductor, the β''-$(ET)_2SF_5CHFSO_3$ metallic material, and the 50:50 superconductor/metal composite in the $\vec{E} \perp b$ polarization. Inset: close-up view of the vibrational response of the same three materials on an absolute scale.

Among others, this yields the frequency-dependent conductivity, $\sigma_1(\omega)$, which provides information on the lossy response of the sample.

III. Results

A. Spatial Disorder: Superconductor/Metal Composites. Figure 4 shows the 300 K optical conductivity of the β''-$(ET)_2SF_5CH_2CF_2SO_3$ superconductor, the β''-$(ET)_2SF_5CHFSO_3$ metal, and the 50:50 SC/M mixed crystal. This set of materials allows exploration of spatial disorder. Despite the structural difference between the two anions (R = CH_2CF_2 and CHF), the anion pocket is ordered in both cases. We concentrate on the $E \perp b$ (intrastack) directed spectra because those in the conducting direction are identical, independent of anion character.[47] Low-energy electronic excitations are clearly observed at ≈5200 and 9600 cm^{-1} in the spectrum of the 50:50 composite. Spectra of the 25:75 and 75:25 composites (not shown) display similar features with reduced intensity. In the spectra of the superconductor (100:0) and metal (0:100), there is only a slight hint of the 5200-cm^{-1} excitation. There is no evidence of the 9600-cm^{-1} feature in the superconducting material. The inset to Figure 4 shows a close-up view of the vibrational features, discussed in detail later in this section.

To better illustrate the effects of spatial disorder on the electronic properties, we plot the intensities of the two low-energy electronic excitations at 5200 and 9600 cm^{-1} as a function of chiral (R = CHF) anion concentration in the superconducting matrix. As shown in Figure 5, the ≈5200- and 9600-cm^{-1} excitations grow with increasing anion substitution and then diminish again; the peak intensities are strongest at the 50:50 SC/M composition, exactly where the spatial disorder is a maximum. In addition to the aforementioned intensity effect, the 9600-cm^{-1} excitation displays a small red

(47) There are several reasons to concentrate on spectra in the low-conductivity direction. First, the $E \parallel b$ spectra are nearly identical, independent of anion concentration. Second, the $E \parallel b$ spectra of the pristine superconductor, metal−insulator, and metallic samples were reported previously.[34−36] Theoretical work suggests that the electrodynamic response in the transverse direction of layered solids is the most important for influencing superconductivity.[53] The $E \perp b$ direction corresponds to that of thelow-dimensional ET stack.

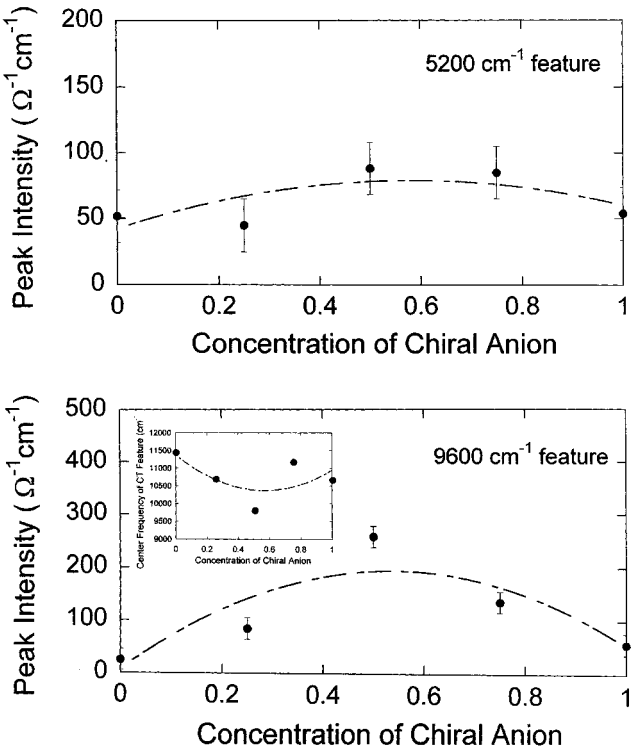

Figure 5. Top panel: intensity of the ≈5200-cm^{-1} charge-transfer feature as a function of chiral anion concentration for the SC/M composite system. Bottom panel: intensity of the ≈9600-cm^{-1} charge-transfer feature as a function of chiral anion concentration for the SC/M composite system. Inset: center frequency of ≈9600-cm^{-1} charge-transfer feature as a function of chiral anion concentration for the SC/M composites.

shift with increasing "impurity concentration," as shown in the inset of Figure 5, reaching a minimum at the 50:50 composition. This suggests that the ET stack polarized excitation is most facile with maximum spatial disorder.

The data in Figures 4 and 5 clearly demonstrate that the ≈5200- and 9600-cm^{-1} low-energy excitations in the β″-(ET)$_2$SF$_5$RSO$_3$ system are symptomatic of spatial disorder resulting from anion substitution. But what are the microscopic origins of these excitations? On the basis of the characteristic energy, width, shape, and polarization direction,[48−50] we assign the 5200- and 9600-cm^{-1} features as charge-transfer excitations along the ET stack,[36] for instance, ET^0 + ET* → ET* + ET^0. Such bands have been extensively studied in a number of organic molecular solids and are well-known to appear in the chain-directed spectral response.[48−50] As discussed in more detail later, these charge-transfer excitations are very sensitive to electronic localization caused by random variations in the anion potential on the ET stack.

Figure 6 displays the 300 K polarized middle infrared reflectance spectra of the β″-(ET)$_2$SF$_5$CH$_2$CF$_2$SO$_3$ superconductor, the β″-(ET)$_2$SF$_5$CHFSO$_3$ metal, and a series (75:25, 50:50, and 25:75) of SC/M composite samples. As described in detail below, the vibrational

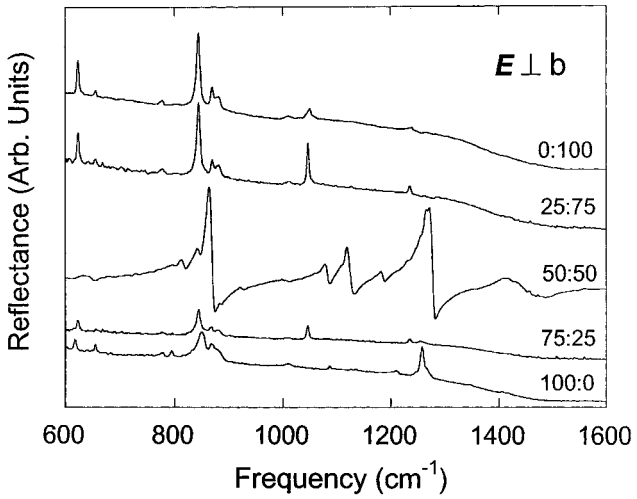

Figure 6. 300 K reflectance spectra of the β″-(ET)$_2$SF$_5$CH$_2$CF$_2$SO$_3$ superconductor, the β″-(ET)$_2$SF$_5$CHFSO$_3$ metal, and the 75:25, 50:50, and 25:75 superconductor/metal composites in the $E \perp b$ polarization. The curves are offset for clarity.

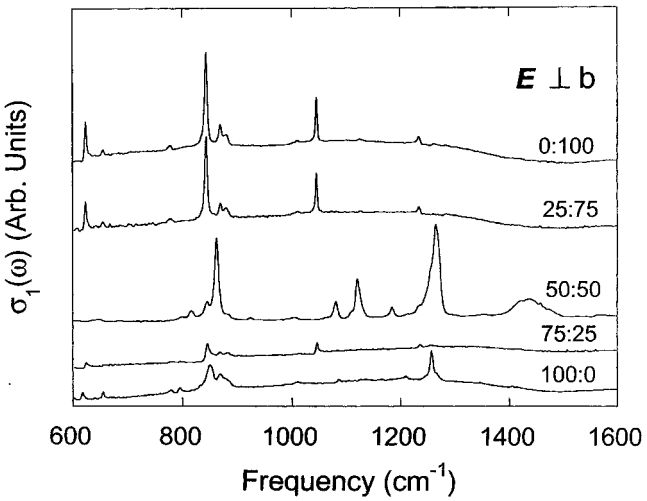

Figure 7. 300 K frequency-dependent conductivity of the β″-(ET)$_2$SF$_5$CH$_2$CF$_2$SO$_3$ superconductor, the β″-(ET)$_2$SF$_5$CHFSO$_3$ metal, and the 75:25, 50:50, and 25:75 superconductor/metal composites in the $E \perp b$ polarization. The curves are offset for clarity.

response of the SC/M composites perfectly mirrors changes in the aforementioned electronic excitations. The spectral character varies from weakly metallic to semiconducting to weakly metallic again, depending on the anion composition in the composite. The reflectance spectrum for the 50:50 SC/M sample is characteristic of a one-dimensional semiconductor with sharp, strong vibrational modes and a low, flat electronic background. These features give way to weaker phonons and an overdamped electronic response on approach to the 100:0 and 0:100 superconducting and metallic samples, respectively.

The 300 K frequency-dependent conductivity of the β″-(ET)$_2$SF$_5$CH$_2$CF$_2$SO$_3$ superconductor, the β″-(ET)$_2$SF$_5$CHFSO$_3$ metal, and various SC/M composites (75:25, 50:50, and 25:75) is shown in Figure 7. These data illustrate the vibrational differences between the superconductor ($T_c \sim 5.2$) and the "damaged" materials. For instance, the 1250-cm^{-1} mode in the superconductor, assigned as C−F stretching in the anion, is absent

(48) Tanner, D. B. In *Extended Linear Chain Compounds*; Miller, J. S., Ed.; Plenum Publishing Corp.: New York, 1982; Vol. 2, Chapter 5.
(49) Jacobsen, C. S. In *Semiconductors and Semi-Metals*; Conwell, E. M., Ed.; Academic Press: New York, 1985; Vol. 27, Chapter 5.
(50) Yarsev, Y. M.; Swietlik, R. *Rev. Solid State Sci.* **1990**, *4*, 69.

in the 75:25 composite, indicating that internal anion/ET interactions are the first to be destroyed upon introduction of spatial disorder. At the same time, the weak structure at 1050 cm^{-1} in the 75:25 composite is not present in the spectrum of the superconductor. The vibrational mode at 850 cm^{-1} (assigned as $^{-}SF_5$ stretching in the anion) is present in both samples, with only a slight variation. The more distinct vibrational changes between the 75:25 and 50:50 composites include a major shape variation and blue shifting of the 850- and 1050-cm^{-1} structures as well as new modes at 1150 and 1200 cm^{-1} in the 50:50 sample. The 1250-cm^{-1} mode is very intense. A broad structure near 1450 cm^{-1} is also observed. The response of the 25:75 composite is most similar to that of the 75:25 material, with peaks at 850 and 1050 cm^{-1}, although the modes of the 75:25 composite are more pronounced than those in the 25:75 sample. The vibrational modes of the 25:75 composite and metallic (R = CHF) sample are nearly identical. One small difference includes the appearance of a new structure at 650 cm^{-1}, seen clearly in the two samples with the highest $SF_5CHFSO_3^-$ anion concentrations. The intense 1150- and 1200-cm^{-1} vibrations in the 50:50 sample are not present in either the 25:75 composite or metal. Note that the overdamped electronic background is slightly more pronounced in the 0:100 M compared to that of the 100:0 SC. There is no low-energy electronic background in the 50:50 composite, typical of a low-dimensional semiconductor; strong charge-transfer excitations (≈5200 and 9600 cm^{-1}) are observed (Figure 4), reflecting a transfer of oscillator strength to higher energy.

B. Local Disorder: *β″*-(ET)$_2$SF$_5$CHFCH$_2$SO$_3$. To gain additional insight into local disorder in the *β″* family of materials and the spectral signature of disorder in the SC/MI composites, we briefly revisit our most important results on the *β″*-(ET)$_2$SF$_5$CHFCF$_2$SO$_3$ metal/insulator material. The main differences between the spectrum of the MI and SC materials are observed in the least conducting direction[47] and include two low-energy electronic features at ≈5200 and 9600 cm^{-1}.[35] Band structure calculations cannot account for these excitations;[35,36,51] thus, they peaked our interest and originally motivated this work. Originally interpreted as possible correlation effects, the 5200- and 9600-cm^{-1} charge-transfer excitations were tentatively associated with disorder because of introduction of the chiral anion and the resulting disruption in the long-range hydrogen bonding inside the anion pocket.[36] In the pristine metal−insulator material, there is only local (anion pocket) disorder; therefore, spectroscopic studies of this system show that local orientational disorder alone is sufficient to cause localized charge-transfer excitation in the ET stack.

C. Combined Spatial and Anion Pocket Disorder: Superconductor/Metal−Insulator Composites. The main panel of Figure 8 shows the 300 K $\vec{E} \perp b$ optical conductivity of the *β″*-(ET)$_2$SF$_5$CH$_2$CF$_2$SO$_3$ superconductor, the *β″*-(ET)$_2$SF$_5$CHFCF$_2$SO$_3$ metal−insulator, and the 50:50 SC/MI mixed crystal material. This set of materials allows simultaneous exploration of both spatial and local disorder. Spatial disorder is maximized at the 50:50 composition, whereas local disorder grows with increasing levels of substitution and is maximum at 0:100, in the pristine metal−insulator material. As before, we concentrate on the $\vec{E} \perp b$ (intrastack) data because all spectra along the highly conducting direction are virtually identical.[47] Low-energy electronic excitations are observed near ≈5200 and 9600 cm^{-1} for the 0:100 material and the 50:50 SC/MI composite; in the superconducting sample (R = CH_2CF_2) only a slight indication of the 5200-cm^{-1} feature is observed. The intensity of these electronic excitations seems to vary gradually, albeit nonlinearly, across composition space, despite the aforementioned competition between local and spatial effects. The 5200- and 9600-cm^{-1} excitations of pristine *β″*-(ET)$_2$SF$_5$CHFCF$_2$SO$_3$ (the MI sample) display the greatest intensity; this sample has maximum local anion pocket disorder, but no spatial disorder. The inset of Figure 8 shows a close-up view of the vibrational features, discussed in detail later in this section.

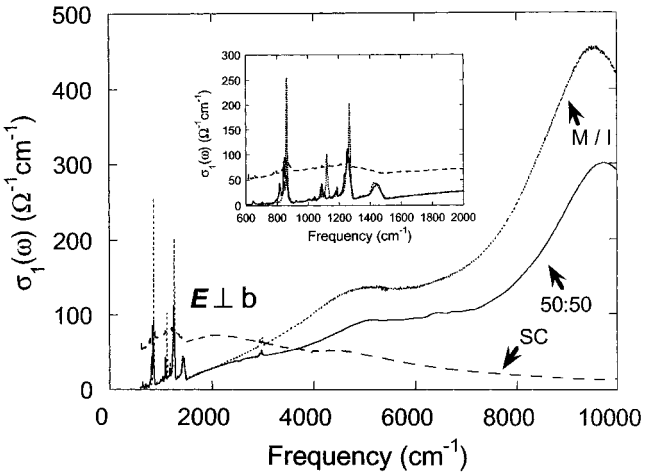

Figure 8. 300 K optical conductivity of the *β″*-(ET)$_2$SF$_5$CH$_2$CF$_2$SO$_3$ superconductor, the *β″*-(ET)$_2$SF$_5$CHFCF$_2$SO$_3$ metal−insulator material, and the 50:50 superconductor/metal−insulator composite in the $\vec{E} \perp b$ polarization. Inset: close-up view of the vibrational response of the same three materials on an absolute scale.

To quantify the trend in the two electronic excitations (5200 and 9600 cm^{-1}) in the SC/MI composites, the peak intensities are plotted as a function of chiral anion concentration in the superconducting matrix. Figure 9 illustrates that excitation intensities grown with increasing R = $CHFCF_2$ incorporation. The intensity growth is nonlinear in the middle of the composition range and may reflect the combined effects of spatial and local (anion pocket) disorder in the SC/MI composites (Table 1). In addition, the 9600-cm^{-1} excitation displays a small redshift with increasing amounts of chiral anion, pulling back again above the 25:75 composite composition (inset of the bottom panel, Figure 9). This suggests that localization is strongest with substantial, but not necessarily full, chiral anion incorporation.

Figure 10 shows a close-up view of the 300 K polarized middle infrared reflectance spectrum of the *β″*-(ET)$_2$SF$_5$CH$_2$CF$_2$SO$_3$ superconductor, the *β″*-(ET)$_2$SF$_5$CHFCF$_2$SO$_3$ metal−insulator, and a series (75:25, 50:50, and 25:75) of SC/MI mixed crystals. In these SC/MI composites, the vibrational features change smoothly across composition space, despite the competing spatial and local

(51) Koo, H.-J.; Whangbo, M.-H.; Dong, J.; Olejniczak, I.; Musfeldt, J. L.; Schlueter, J. A.; Geiser, U. *Solid State Commun.* **1999**, *112*, 403.

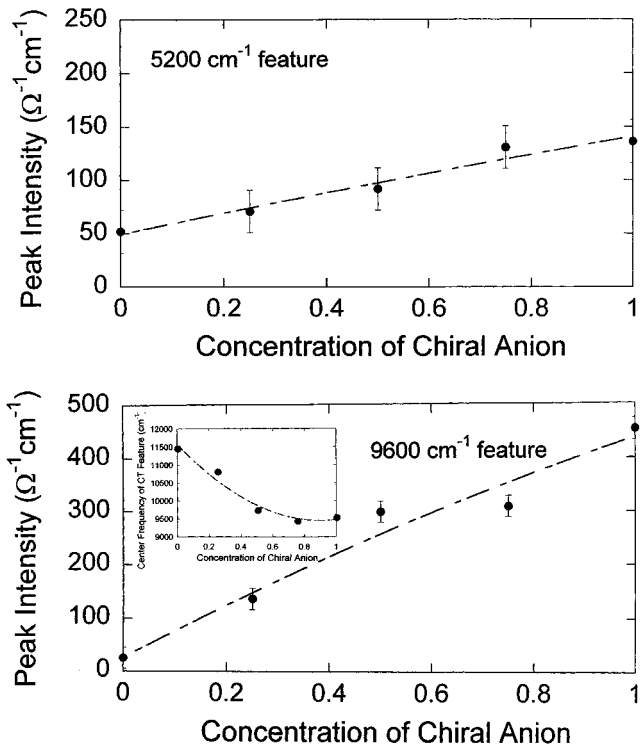

Figure 9. Top panel: intensity of the ≈5200-cm^{-1} charge-transfer feature as a function of chiral anion concentration for the SC/MI composite system. Bottom panel: intensity of the ≈9600-cm^{-1} charge-transfer feature as a function of chiral anion concentration for the SC/MI composite system. Inset: center frequency of ≈9600-cm^{-1} charge-transfer feature as a function of chiral anion concentration for the SC/MI composites.

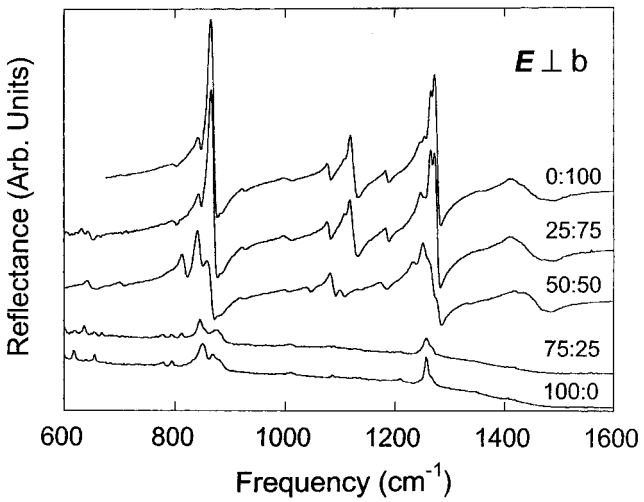

Figure 10. 300 K reflectance spectra of the β″-(ET)$_2$SF$_5$CH$_2$CF$_2$SO$_3$ superconductor, the β″-(ET)$_2$SF$_5$CHFCF$_2$SO$_3$ metal−insulator, and the 75:25, 50:50, and 25:75 superconductor/metal−insulator composites in the $\bar{E} \perp b$ polarization. The curves are offset for clarity.

disorder effects over most of the composition range. The superconductor displays modest vibrational features superimposed on a weakly metallic background, whereas the metal/insulator material shows strong and well-resolved modes and a semiconducting electronic response. As described below, the vibrational response of the SC/MI composites follows changes in the low-energy electronic excitations. In particular, several width changes and splittings may be connected with disorder.

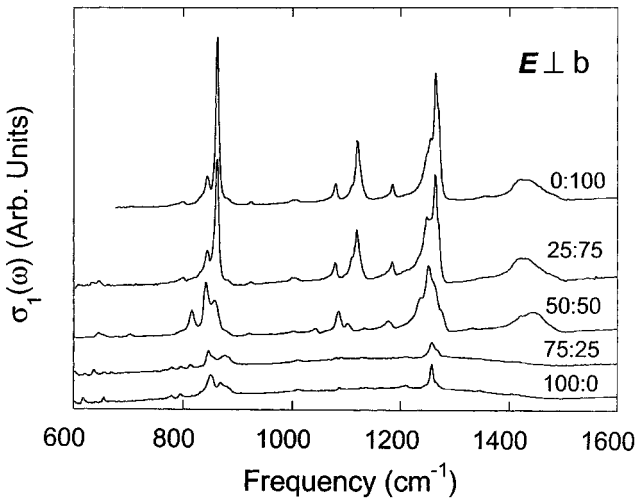

Figure 11. 300 K frequency-dependent conductivity of the β″-(ET)$_2$SF$_5$CH$_2$CF$_2$SO$_3$ superconductor, the β″-(ET)$_2$SF$_5$CHFCF$_2$SO$_3$ metal−insulator, and the 75:25, 50:50, and 25:75 superconductor/metal−insulator composites as a function of frequency in the $\bar{E} \perp b$ polarization. The curves are offset for clarity.

Figure 11 displays a close-up view of the frequency-dependent conductivity of the β″-(ET)$_2$SF$_5$CH$_2$CF$_2$SO$_3$ SC, the β″-(ET)$_2$SF$_5$CHFCF$_2$SO$_3$ MI, and a series (75:25, 50:50, and 25:75) of SC/MI composites. There are only minimal changes in the vibrational response between the superconductor and 75:25 composite; for instance, the 1250-cm^{-1} excitation, attributed to C−F stretching in the anion, is less well-defined in the 75:25 composite. More dramatic spectral changes are observed between the 75:25 and 50:50 compositions. For example, the 850- and 1250-cm^{-1} modes are much broader in the 50:50 composite; a new feature appears at 1100 cm^{-1}. Additionally, a broad structure forms at 1450 cm^{-1} for the 50:50 composite, which remains in the 25:75 and 0:100 spectra. Other important changes are observed in the vibrational modes of the 25:75 composite. For instance, the feature at 850 cm^{-1} becomes more unevenly split and blue-shifts considerably (indicating microscopically more similar $^{-}SF_5$ interactions). Phonons at 1100 and 1250 cm^{-1} also become sharper and more pronounced. The pristine MI sample displays very strong vibrational features, as detailed earlier.[35]

IV. Discussion

On the basis of the intensity, width, and polarization direction,[48−50] we assign the ≈5200- and 9600-cm^{-1} spectral features in the SC/M and SC/MI composites as charge-transfer excitations along the ET stack. These charge-transfer excitations appear in the spectra because of both spatial and local disorder, which result in increased localization compared to that in the superconducting material (β″-(ET)$_2$SF$_5$CH$_2$CF$_2$SO$_3$). The 5200- and 9600-cm^{-1} excitations grow and diminish together, depending on the composite composition. This indicates that these excitations are induced by a similar mechanism and correlated in a microscopic way. Local disorder is, however, clearly more effective than positional disorder in creating oscillator strength.

A. Superconductor/Metal Composites. The SC/M mixed crystals exhibit only spatial disorder. If the

$SF_5RSO_3^-$ anions are clustered in large domains in the crystals, substantial variations in the anion potential are not expected; in this case, electronic localization and the resulting charge-transfer bands should be weak. In contrast, the 50:50 SC/M composite displays pronounced charge-transfer excitations. This suggests that the 50:50 composite has nearly alternating positional disorder (Table 1), consistent with statistical expectations for mixed anion incorporation. Larger positional length scales are expected on moving away from the 50:50 composition. That the larger domain size reduces variations in the anion potential is evident in the spectral trends of the 25:75 and 75:25 SC/M materials.

The minute differences in electronic structure between the superconductor ($R = CH_2CF_2$) and the metallic ($R = CHF$) samples can also be understood in terms of the effect of the anion potential on charge localization in the ET stack.[52] Two facts are pertinent here. First, the anion pocket is substantially smaller in the metallic sample (0:100) than in the superconducting material (100:0).[53] Second, X-ray measurements show that the $R = CHF$ anion displays large thermal ellipsoids.[36,53] Thus, the large anion group thermal motion in the metallic sample may be responsible for slightly localizing charge and preventing superconductivity in β''-$(ET)_2SF_5CHFSO_3$. We anticipate that the thermally broadened, fluctuating potential gives rise to the weak charge-transfer excitations at 5200 and 9600 cm^{-1} in the metallic material (Figure 4). From the absence of the 9600-cm^{-1} excitation in β''-$(ET)_2SF_5CH_2CF_2SO_3$, it is tempting to suggest that removal of the conditions conducive to charge-transfer excitation is necessary to establish superconductivity.

B. Metal−Insulator Material. The β''-$(ET)_2SF_5CH_2CF_2SO_3$ metal−insulator material contains only orientational disorder in the anion pocket because of the chiral nature of the counterion. Here, this local disorder introduces a large-amplitude, small length-scale disorder in the anion layer. The 5200- and 9600-cm^{-1} charge-transfer excitations are enhanced in the spectra by this random potential, which gives rise to electronic localization in the ET stack.

C. Superconductor/Metal−Insulator Composites. The SC/MI mixed crystals contain both spatial and local disorder, which compete over the majority of the composition range. The superposition of these effects results in somewhat irregular, large-amplitude variations in the anion potential. These variations likely occur over a very small length scale.

Spatial and local disorder are maximized in the 50:50 SC/M and 0:100 SC/MI composite systems, respectively. On the basis of relative charge-transfer band intensities (Figures 4 and 8), local orientational disorder effects are much stronger than positional effects—nearly twice as effective at creating oscillator strength at 5200 and 9600 cm^{-1}. This is because the anion pocket disorder results in large-amplitude modulations of the potential, which are very effective in localizing charge on the ET stack.

V. Conclusion

We report 300 K polarized infrared reflectance measurements on β''-$(ET)_2SF_5RSO_3$ solid solutions ($R = CH_2CF_2$, CHF, $CHFCF_2$). Both SC/M and SC/MI materials were prepared, allowing us to investigate the separate and combined effects of both spatial (positional) and local (anion pocket) disorder. We find that two low-energy electronic transitions, observed along the stacking direction at ≈5200 and 9600 cm^{-1}, are enhanced in the spectra with both spatial and local disorder. These excitations are due to electron localization and subsequent charge transfer on ET dimers and are driven by random variations of the anion potential. These results are important for the understanding of superconductivity in organic solids and may be relevant to understanding middle infrared charge localization in some of the layered transition-metal oxides as well.

Acknowledgment. This work was supported at the University of Tennessee and SUNY—Binghamton by Grants DMR-0139414 and DMR-0196473 from the Division of Materials Research at the National Science Foundation. The international aspects of the project were funded by the Division of International Programs (Grant INT-0086475) at the National Science Foundation. Work at North Carolina State University and Argonne National Laboratory was supported by the Office of Basic Energy Science, Division of Material Sciences, U.S. Department of Energy, under Grants DE-FG05-86ER45259 and W-31-109-ENG-38. Research at Portland State University was supported by NSF Grant CHE-9904316 and the Petroleum Research Fund ACS-PRF 34624-AC7. We thank P. A. Varughese for technical assistance.

CM010378B

(52) That the 9600-cm^{-1} excitation is not observed in the β''-$(ET)_2SF_5CH_2CF_2SO_3$ materials seems to be key to establishing superconductivity.

(53) Mazumdar, S.; Clay, R. T.; Campbell, D. K. *Phys. Rev. B* **2000**, *62*, 13400.